IEEE Access
Multidisciplinary ⋮ Rapid Review ⋮ Open Access Journal

Received May 4, 2020, accepted May 21, 2020, date of publication June 2, 2020, date of current version June 15, 2020.

Digital Object Identifier 10.1109/ACCESS.2020.2999372

Design of a Spatial Vibration System for Prescribed Ratio of Energy Peaks

YEONG GEOL LEE AND YONG JE CHOI
Department of Mechanical Engineering, Yonsei University, Seoul 03722, South Korea
Corresponding author: Yong Je Choi (yjchoi@yonsei.ac.kr)

This work was supported by the Basic Science Research Program through the National Research Foundation of Korea (NRF) funded by the Ministry of Education under Grant 2018R1D1A1B07048708.

ABSTRACT The work ratio is a primary factor in the applications relevant to wide bandwidth requirements because a bandwidth depends on resonant peaks. Especially, since a single-body system can have up to six resonant peaks, a six degree-of-freedom spatial system is more desirable for a broad bandwidth design. This paper presents a novel design method of a spatial vibration system for any prescribed ratio of energy peaks. Firstly, we introduce an important and concise geometric nature of a spatial vibration system with a single rigid body when it has only rotational vibration modes. The vibration modes represent vibration axes and six lines of action can be obtained by transforming the vibration modes by the mass matrix. It is shown that the six axes of vibration and six lines of action form two orthocentric tetrahedra that share the orthocenter coincident with the mass center. It is also shown that the stiffness matrix determined from two tetrahedra can always be realized by means of parallel connection of line springs. Using the orthocentric tetrahedra, we acquire analytical expressions for the energy produced by external forces at resonant frequencies, which is used to determine vibration modes that satisfy the requirements for given mass properties and six target resonant frequencies. Finally, the stiffness matrix that satisfies requirements is found and realized. To illustrate the process of the presented method, we use four numerical examples with different work ratios and demonstrate that the method is useful for a wide bandwidth.

INDEX TERMS Broad bandwidth, spatial vibration system, resonant frequency, rotational vibration mode, work ratio.

I. INTRODUCTION

When designing vibration systems such as vibration-based energy harvesters and vibration absorbers, the magnitudes of resonant peaks are considered more important because the bandwidth is affected by the magnitudes of peaks. It has been known that the specific ratio of energy peaks allows for a vibration system to have a broad bandwidth [1]. Thus, the ratio of the resonant peaks should be considered in the design stage of a vibration system which requires a wide bandwidth.

For a multimodal system, it is difficult to tune the magnitudes of resonant peaks to suit requirements because they depend on both vibration modes and resonant frequencies. Furthermore, when designing a vibrating system, vibration modes must be specified so that they satisfy orthogonality with respect to the mass matrix and a spatial stiffness matrix designed for given requirements should satisfy realization condition since the stiffness matrix is not always realizable [2]. These constraints complicate the design of a spatial vibration system.

To overcome the complexity, some researchers suggested a system consisting of one degree-of-freedom (DOF) beam-mass systems [3], [4]. Since 1-DOF systems are independent, the magnitude of a peak of each system can be easily tuned. Another approach is to design a 3-DOF planar vibration system. There are two advantages of the design using a planar system. First, there is a transparent geometric property that three vibration centers form a triangle of which the orthocenter is coincident with the center of mass [5]. Second, a planar stiffness matrix with rank 3 can always be realized by using either parallel connection of line springs or serial connection of torsion springs [6]. Kim *et al.* [1] utilized those advantages to develop a design method of a 3-DOF vibration system for prescribed work ratios. This method was applied to the design of a vibration energy harvester composed of serial

The associate editor coordinating the review of this manuscript and approving it for publication was Tao Wang.

linkages [7], [8]. However, since a rigid body has 6-DOF in space, it may be said that a 6-DOF spatial system is more desirable for high efficiency.

A vibration mode of a spatial system can be viewed as a repetitive small screw motion [9]. This complex motion gives rise to complicated geometric relations among vibration modes. Some researchers have made efforts to find the conditions that simplify the geometric characteristics of a spatial vibration system. Representatively, the conditions for plane(s) of symmetry were discovered and presented in [10]–[13]. If a vibrating system has a plane of symmetry, the vibration modes are decoupled into in-plane and out-of-plane vibration modes, which refer to rotational vibrations whose axes are perpendicular to the plane of symmetry and lying on the plane, respectively. Jang *et al.* [14] derived the geometric relations between in- and out-of-plane vibration modes from orthogonality with respect to the mass matrix. Recently, Lee *et al.* [15] proposed a new development of geometric conditions for a vibration system to have only rotational modes. They also showed that there exist three configurations of vibration axes with simple geometry.

In order to develop a design method of a spatial vibration system with a realizable stiffness matrix, we utilize one of three configurations of vibration axes presented in [15]. Using the geometric relations between vibration modes, we develop a systematic design method for prescribed ratios of energy peaks at six target resonance frequencies. It will be shown that the stiffness matrix synthesized using this method can always be realized by means of parallel connection of line springs.

This paper is organized as follows: Section II explains theoretical preliminaries. Section III describes geometrical relationships between vibration modes found from orthogonality with respect to the mass matrix. It is also shown that the synthesized stiffness matrix is realizable. In section IV, we present the design method of both direct and base excitation systems. Section V illustrates numerical examples with demonstration of usefulness of the proposed method. A conclusion is given in the final section.

II. PRELIMINARIES

A. GEOMETRIC REPRESENTATION OF VIBRATION MODES

We consider a rigid body supported by two sets of line springs (Fig. 1): 1) one set of n springs intersecting at the point A and 2) the other set of n springs lying on the plane P for $n \geq 3$. Then, a symmetric and positive definite rank 6 stiffness matrix $\boldsymbol{K}$ $\left(\in R^{6\times 6}\right)$ can be expressed as [16]–[18]

$$\begin{aligned}\boldsymbol{K} &= \boldsymbol{K}_1 + \boldsymbol{K}_2 = \boldsymbol{j}_1\boldsymbol{k}_1\boldsymbol{j}_1 + \boldsymbol{j}_2\boldsymbol{k}_2\boldsymbol{j}_2 \\ &= \sum_{i=1}^{n} k_{\alpha i}\widehat{\boldsymbol{\alpha}}_i\widehat{\boldsymbol{\alpha}}_i^T + \sum_{i=1}^{n} k_{\beta i}\widehat{\boldsymbol{\beta}}_i\widehat{\boldsymbol{\beta}}_i^T, \end{aligned} \tag{1}$$

where $\boldsymbol{j}_1$ and $\boldsymbol{j}_2$ are $6 \times n$ Jacobian matrices with rank 3

$$\boldsymbol{j}_1 = \begin{bmatrix} \widehat{\boldsymbol{\alpha}}_1 & \cdots & \widehat{\boldsymbol{\alpha}}_n \end{bmatrix} \quad \text{and} \quad \boldsymbol{j}_2 = \begin{bmatrix} \widehat{\boldsymbol{\beta}}_1 & \cdots & \widehat{\boldsymbol{\beta}}_n \end{bmatrix} \tag{2}$$

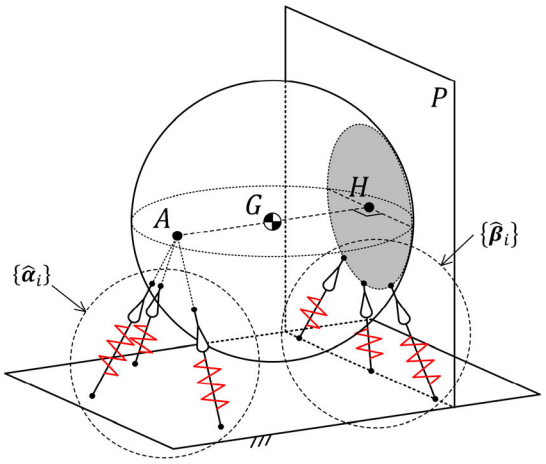

FIGURE 1. Spatial vibration system consisting of two sets of line springs.

and $\boldsymbol{k}_1$ and $\boldsymbol{k}_2$ are $n \times n$ diagonal matrices

$$\boldsymbol{k}_1 = \begin{bmatrix} k_{\alpha 1} & & \boldsymbol{0} \\ & \ddots & \\ \boldsymbol{0} & & k_{\alpha n} \end{bmatrix} \quad \text{and} \quad \boldsymbol{k}_2 = \begin{bmatrix} k_{\beta 1} & & \boldsymbol{0} \\ & \ddots & \\ \boldsymbol{0} & & k_{\beta n} \end{bmatrix}. \tag{3}$$

Each column $\widehat{\boldsymbol{\alpha}}_i$(or $\widehat{\boldsymbol{\beta}}_i$) of $\boldsymbol{j}_1$(or $\boldsymbol{j}_2$) represents a line of action of a force produced by the line spring with the spring constant $k_{\alpha i}$(or $k_{\beta i}$). The lines of action $\widehat{\boldsymbol{\alpha}}_i$ and $\widehat{\boldsymbol{\beta}}_i$ are unit line vectors (of zero pitch), or simply lines, expressed in (Plücker's) ray co-ordinates

$$\widehat{\boldsymbol{\alpha}}_i = \begin{Bmatrix} \boldsymbol{s}_{\alpha i} \\ \boldsymbol{r}_{\alpha i} \times \boldsymbol{s}_{\alpha i} \end{Bmatrix} \quad \text{and} \quad \widehat{\boldsymbol{\beta}}_i = \begin{Bmatrix} \boldsymbol{s}_{\beta i} \\ \boldsymbol{r}_{\beta i} \times \boldsymbol{s}_{\beta i} \end{Bmatrix}, \tag{4}$$

where $\boldsymbol{s}_{\alpha i}$(or $\boldsymbol{s}_{\beta i}$) and $\boldsymbol{r}_{\alpha i}$(or $\boldsymbol{r}_{\beta i}$) denote the unit direction and position vector to a point on the line of action $\widehat{\boldsymbol{\alpha}}_i$(or $\widehat{\boldsymbol{\beta}}_i$). It is noted here that $\widehat{\boldsymbol{\alpha}}_i$'s and $\widehat{\boldsymbol{\beta}}_i$'s are respectively the lines of action intersecting at the point A and lying on the plane P (Fig. 1). Clearly, the line vectors satisfy the following relation:

$$\widehat{\boldsymbol{\alpha}}_i^T \boldsymbol{\Delta} \widehat{\boldsymbol{\alpha}}_i = \widehat{\boldsymbol{\beta}}_i^T \boldsymbol{\Delta} \widehat{\boldsymbol{\beta}}_i = 0, \tag{5}$$

where $\boldsymbol{\Delta} = \begin{bmatrix} \boldsymbol{0}_{3\times 3} & \boldsymbol{I}_{3\times 3} \\ \boldsymbol{I}_{3\times 3} & \boldsymbol{0}_{3\times 3} \end{bmatrix}$. From (5), the trace of $\boldsymbol{K}\boldsymbol{\Delta}$ becomes zero:

$$\text{tr}\,(\boldsymbol{K}\boldsymbol{\Delta}) = \sum_{i=1}^{n} \left(k_{\alpha i}\widehat{\boldsymbol{\alpha}}_i^T \boldsymbol{\Delta} \widehat{\boldsymbol{\alpha}}_i + k_{\beta i}\widehat{\boldsymbol{\beta}}_i^T \boldsymbol{\Delta} \widehat{\boldsymbol{\beta}}_i \right) = 0. \tag{6}$$

This means that $\boldsymbol{K}$ can be realized by means of parallel connection of line springs when $\boldsymbol{K}$ satisfies (6) [2].

Now, the equation of motion for undamped free vibration can be given by

$$\boldsymbol{M}\ddot{\boldsymbol{X}} + \boldsymbol{K}\boldsymbol{X} = \boldsymbol{0}, \tag{7}$$

where $\boldsymbol{M}$ is 6×6 mass matrix. A small harmonic displacement can be expressed as

$$\boldsymbol{X} = \widehat{\boldsymbol{X}} e^{j\omega t}, \tag{8}$$

where $\widehat{\boldsymbol{X}}$ is a screw expressed in (Plücker's) axis co-ordinates. Using (7) and (8), we have:

$$\left(\boldsymbol{K} - \omega^2 \boldsymbol{M}\right) \widehat{\boldsymbol{X}} = 0. \tag{9}$$

From (9), we obtain the natural frequencies $\omega_i (i = 1, \ldots, 6)$ and the corresponding vibration modes $\widehat{\boldsymbol{X}}_i (i = 1, \ldots, 6)$. As illustrated in Fig. 1, we assume that the vibration system satisfies the following two conditions:

1) The moments of inertia about all the principal axes are identical (e.g. a sphere-shaped rigid body).
2) The mass center G is internal division of $\overline{AH}$ and $\overline{AG} \cdot \overline{GH} = r_g^2$. H is the foot of perpendicular drawn from A to the plane P and r_g is radius of gyration of the rigid body.

Under these assumptions, all the vibration modes become rotational ones [15]. That is, $\widehat{\boldsymbol{X}}_i$'s become line vectors

$$\widehat{\boldsymbol{X}}_i = \begin{Bmatrix} \boldsymbol{r}_i \times \boldsymbol{s}_i \\ \boldsymbol{s}_i \end{Bmatrix}, \tag{10}$$

where $\boldsymbol{s}_i$ and $\boldsymbol{r}_i$ denote respectively the unit direction and position vector to a point on the axis of $\widehat{\boldsymbol{X}}_i$. Furthermore, the vibration axes can be grouped into two sets (Fig. 2): 1) one set of three axes intersecting at the point A and 2) the other set of three axes lying on the plane P. This configuration of vibration axes is used to derive the design method in this paper. It is noted that the white and black arrowheads in all the figures depict the line vectors expressed in ray and axis co-ordinates, respectively.

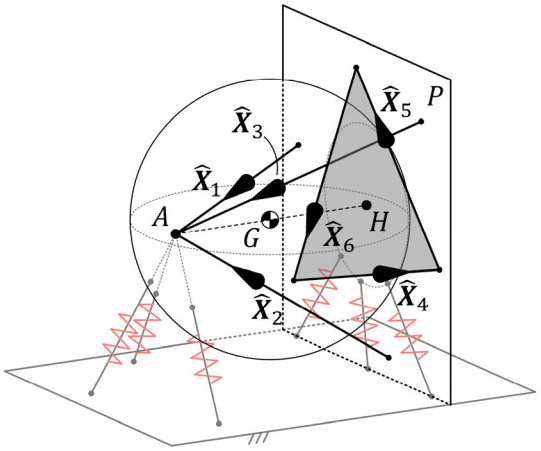

FIGURE 2. Two groups of vibration axes.

B. DESIGN EQUATION

The design equation can be derived from orthogonality of a vibration system. Orthogonal characters with respect to the mass and stiffness matrices are given by

$$\boldsymbol{S}^T \boldsymbol{M} \boldsymbol{S} = \begin{bmatrix} \tilde{m}_1 & & \boldsymbol{0} \\ & \ddots & \\ \boldsymbol{0} & & \tilde{m}_6 \end{bmatrix} \tag{11}$$

and

$$\boldsymbol{S}^T \boldsymbol{K} \boldsymbol{S} = \begin{bmatrix} \tilde{k}_1 & & \boldsymbol{0} \\ & \ddots & \\ \boldsymbol{0} & & \tilde{k}_6 \end{bmatrix}, \tag{12}$$

where $\boldsymbol{S} = \left[\widehat{\boldsymbol{X}}_1 \cdots \widehat{\boldsymbol{X}}_6\right]$, $\tilde{m}_i = \widehat{\boldsymbol{X}}_i^T \boldsymbol{M} \widehat{\boldsymbol{X}}_i$, and $\tilde{k}_i = \widehat{\boldsymbol{X}}_i^T \boldsymbol{K} \widehat{\boldsymbol{X}}_i$ for $i = 1, \ldots, 6$. From (11) and (12), we can obtain the following design equation:

$$\boldsymbol{K} = \boldsymbol{M} \boldsymbol{S} \left[\omega^2\right] \boldsymbol{S}^{-1} \tag{13}$$

where $\left[\omega^2\right] = \mathrm{diag}\left(\omega_1^2, \ldots, \omega_6^2\right)$. Equation (13) implies that if the desired natural frequencies are prespecified, the stiffness matrix can be determined by a proper assignment of the modal matrix for the given mass properties of a rigid body. Considering that a vibration mode can be viewed as a geometric element (e.g. a line), from (11), we can obtain new geometric constraints on the two groups of vibration axes for the given inertia matrix.

III. MODAL SYNTHESIS

A. GEOMETRIC CONSTRAINTS ON VIBRATION AXES

To derive the geometric constraints on vibration axes from orthogonality with respect to the mass matrix $\boldsymbol{M}$, we first investigate the geometric properties of $\boldsymbol{M}$ as a linear one-to-one transformation, which maps a screw expressed in axis co-ordinates into one in ray co-ordinates [15]. For the given mass matrix $\boldsymbol{M}$, the mapping of $\boldsymbol{M}$ between two screws is invariant with respect to co-ordinate frame transformations. Thus, if we place the co-ordinate frame so that its origin is coincident with the mass center, then the mass matrix $\boldsymbol{M}$ becomes:

$$\boldsymbol{M} = \mathrm{diag}\left(m, m, m, I, I, I\right), \tag{14}$$

where m is the mass and I denotes the moment of inertia. Transforming the vibration mode $\widehat{\boldsymbol{X}}_i$ by $\boldsymbol{M}$ yields:

$$\boldsymbol{M} \widehat{\boldsymbol{X}}_i = \begin{Bmatrix} m\left(\boldsymbol{r}_i \times \boldsymbol{s}_i\right) \\ I \boldsymbol{s}_i \end{Bmatrix}.$$

If we choose the position vector $\boldsymbol{r}_i$ to be perpendicular to $\boldsymbol{s}_i$, $\boldsymbol{s}_i$ can be denoted by

$$\boldsymbol{s}_i = \frac{1}{r_i^2}\left(-\boldsymbol{r}_i \times \left(\boldsymbol{r}_i \times \boldsymbol{s}_i\right)\right), \tag{15}$$

where $r_i = \|\boldsymbol{r}_i\|$. Using (15), we can rewrite $\boldsymbol{M} \widehat{\boldsymbol{X}}_i$ as

$$\boldsymbol{M} \widehat{\boldsymbol{X}}_i = m r_i \widehat{\boldsymbol{x}}_i, \tag{16}$$

where

$$\widehat{\boldsymbol{x}}_i = \begin{Bmatrix} \boldsymbol{s}_i' \\ \boldsymbol{r}_i' \times \boldsymbol{s}_i' \end{Bmatrix}, \tag{17}$$

The vectors $\boldsymbol{s}_i'$ and $\boldsymbol{r}_i'$ are given by

$$\boldsymbol{s}_i' = \frac{1}{r_i}(\boldsymbol{r}_i \times \boldsymbol{s}_i) \tag{18}$$

and

$$\boldsymbol{r}_i' = -\left(\frac{r_g}{r_i}\right)^2 \boldsymbol{r}_i \tag{19}$$

The observation of (18) and (19) reveals the following geometrical relationships between the mass center and two lines ($\widehat{\boldsymbol{X}}_i$ and $\widehat{\boldsymbol{x}}_i$):

1) The two lines $\widehat{\boldsymbol{X}}_i$ and $\widehat{\boldsymbol{x}}_i$ are perpendicular to each other since $\boldsymbol{s}_i \cdot \boldsymbol{s}_i' = 0$.
2) The mass center lies on the common perpendicular of $\widehat{\boldsymbol{X}}_i$ and $\widehat{\boldsymbol{x}}_i$ since $\boldsymbol{r}_i'$ and $\boldsymbol{r}_i$ are collinear.
3) The distances from the mass center G to two lines $\widehat{\boldsymbol{X}}_i$ and $\widehat{\boldsymbol{x}}_i$ satisfy that $r_i r_i' = r_g^2$ where $r_i' = \|\boldsymbol{r}_i'\|$.

The above relations are illustrated in Fig. 3.

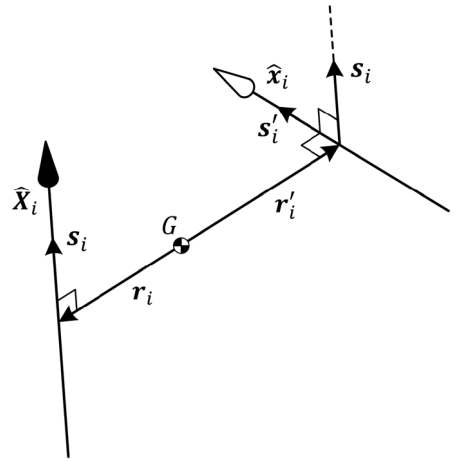

FIGURE 3. Geometrical relation between $\widehat{\boldsymbol{X}}_i$ and $\widehat{\boldsymbol{x}}_i$.

In what follows, the relation between $\widehat{\boldsymbol{X}}_i$ and $\widehat{\boldsymbol{x}}_j$ for $i \neq j$ can be obtained from (11) and (16) as

$$\widehat{\boldsymbol{X}}_i^T \widehat{\boldsymbol{x}}_j = 0 \quad \text{for } i \neq j. \tag{20}$$

When the two lines $\widehat{\boldsymbol{X}}_i$ and $\widehat{\boldsymbol{x}}_j$ satisfy (20), it is said that they are reciprocal to each other. Equation (20) can be expressed geometrically as [9]:

$$\widehat{\boldsymbol{X}}_i^T \widehat{\boldsymbol{x}}_j = -d_{ij} \sin\theta_{ij} \tag{21}$$

where θ_{ij} and d_{ij} are the angle and shortest distance between axes of $\widehat{\boldsymbol{X}}_i$ and $\widehat{\boldsymbol{x}}_j$. Therefore, $\widehat{\boldsymbol{X}}_i$ and $\widehat{\boldsymbol{x}}_j$ for $i \neq j$ must meet or be parallel.

Now, we present the first geometric constraint on vibration axes as follows:

Constraint 1: The two groups of lines ($\widehat{\boldsymbol{X}}_1$, $\widehat{\boldsymbol{X}}_2$, $\widehat{\boldsymbol{X}}_3$, $\widehat{\boldsymbol{x}}_1$, $\widehat{\boldsymbol{x}}_2$, $\widehat{\boldsymbol{x}}_3$) and ($\widehat{\boldsymbol{X}}_4$, $\widehat{\boldsymbol{X}}_5$, $\widehat{\boldsymbol{X}}_6$, $\widehat{\boldsymbol{x}}_4$, $\widehat{\boldsymbol{x}}_5$, $\widehat{\boldsymbol{x}}_6$) construct two corresponding ***orthocentric tetrahedra*** which share the altitude $\overline{AH}$.

A tetrahedron is said to be *orthocentric* when all three pairs of opposite edges are perpendicular. The above statement of *Constraint 1* can be proved as follows: Referring to Fig. 4(a), $\widehat{\boldsymbol{x}}_3$ lies on the plane P since the mass matrix $\boldsymbol{M}$ transforms the lines passing through the point A into the lines lying on the plane P, and vice versa (see APPENDIX in [15]). In addition, it is shown in (20) and (21) that $\widehat{\boldsymbol{x}}_3$ meets both $\widehat{\boldsymbol{X}}_1$ and $\widehat{\boldsymbol{X}}_2$. Similarly, it becomes clear that $\widehat{\boldsymbol{x}}_6$ penetrates the point A and meets both $\widehat{\boldsymbol{X}}_4$ and $\widehat{\boldsymbol{X}}_5$(Fig. 4(b)). Therefore, it can be shown that two tetrahedra that share the altitude $\overline{AH}$ are constructed by two groups of lines ($\widehat{\boldsymbol{X}}_1, \widehat{\boldsymbol{X}}_2, \widehat{\boldsymbol{X}}_3, \widehat{\boldsymbol{x}}_1, \widehat{\boldsymbol{x}}_2, \widehat{\boldsymbol{x}}_3$) and ($\widehat{\boldsymbol{X}}_4, \widehat{\boldsymbol{X}}_5, \widehat{\boldsymbol{X}}_6, \widehat{\boldsymbol{x}}_4, \widehat{\boldsymbol{x}}_5, \widehat{\boldsymbol{x}}_6$), and they are orthocentric since all three pairs of opposite edges ($\widehat{\boldsymbol{X}}_i$ and $\widehat{\boldsymbol{x}}_i$) are perpendicular. The proof is complete.

An important property of the orthocentric tetrahedron is that its four altitudes are always concurrent, and the intersecting point is orthocenter. The second geometric constraint on vibration axes is about the orthocenter and the mass center.

Constraint 2: The tetrahedra share ***orthocenter***, which coincides with the center of mass.

To prove this statement, we consider three planes (P_1, P_2, and P_3) respectively containing the axes of $\widehat{\boldsymbol{X}}_i (i = 1, 2, 3)$ and perpendicular to the opposite edges $\widehat{\boldsymbol{x}}_i (i = 1, 2, 3)$ (Fig. 5). Since P_1 contains the common normal to $\widehat{\boldsymbol{X}}_1$ and $\widehat{\boldsymbol{x}}_1$, the mass center G lies on P_1. Similarly, P_2 and P_3 also contain G, and thus G lies on the altitude $\overline{AH}$ since $\overline{AH}$ is the intersection of P_1, P_2, and P_3. Consequently, we can show that the four altitudes intersect at the mass center G, i.e., G is orthocenter of the tetrahedron. In the similar manner, it can also be shown that G coincides with orthocenter of the tetrahedron formed by $\widehat{\boldsymbol{X}}_i (i = 4, 5, 6)$ and $\widehat{\boldsymbol{x}}_i (i = 4, 5, 6)$. These results complete the proof of *Constraints 2*.

Finally, we present the third geometric constraint about the faces of the tetrahedra.

Constraint 3: The four faces of each tetrahedron are ***acute*** triangles.

To prove this, if we assume that a face has the obtuse angle $\angle BCD$ (Fig. 6), then the orthocenter, or the mass center G is clearly outside of the tetrahedron, and the normal position vectors $\boldsymbol{r}_i$ and $\boldsymbol{r}_i'$ are in the same direction. However, this is contradictory to (19) since $\boldsymbol{r}_i$ and $\boldsymbol{r}_i'$ should be in opposite directions. It concludes that all the faces of the tetrahedron cannot have an obtuse angle. If a face is a right triangle, then G and H coincide with the vertex with the right angle. Since $\overline{AG} \cdot \overline{GH} = r_g^2$, r_g becomes zero or A is infinitely distant from G (and H). Because we only consider a rigid body (not point mass) and the case that vibration axes are finite distant from G in this study, all the faces of the tetrahedra must be acute triangles.

Recalling that three vibration modes of a 3-DOF planar vibration system form an acute modal triangle, the orthocenter of which is coincident with the mass center [1], [5] (Fig. 7). Therefore, the aforementioned geometric properties of the 6-DOF spatial vibration system can be considered an extension of the planar system.

B. SEPARATION AND REALIZATION OF STIFFNESS MATRIX

In order to show that the stiffness matrix synthesized from (13) is always realizable, we separate the stiffness

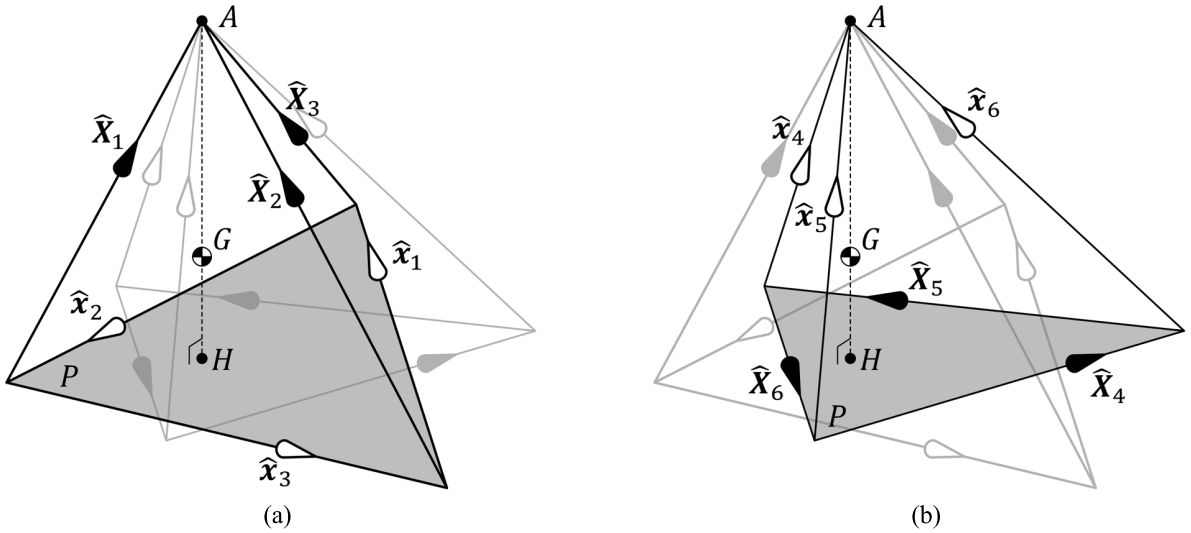

FIGURE 4. Orthocentric tetrahedra formed by vibration axes and lines of action.

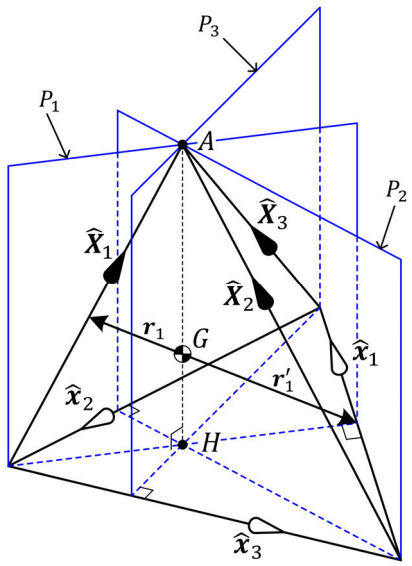

FIGURE 5. Geometrical relationships between the mass center and vibration axes.

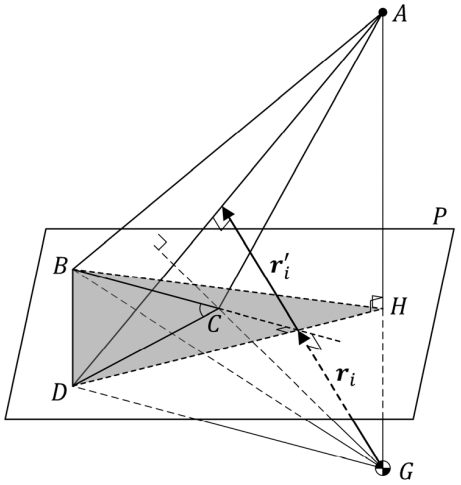

FIGURE 6. Orthocentric tetrahedra of which the face is obtuse.

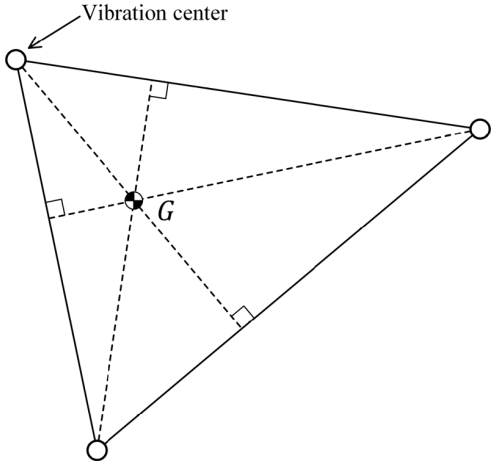

FIGURE 7. Geometric relation between mass and vibration centers in 3-DOF planar system.

matrix $\boldsymbol{K}$ into the sum of two rank 3 matrices in the form of (1). For the given two tetrahedra shown in Fig. 4, the modal matrix $\boldsymbol{S}$ satisfies the following equation:

$$\boldsymbol{S}^T\boldsymbol{S}_r = \begin{bmatrix} \widehat{\boldsymbol{X}}_1^T \\ \vdots \\ \widehat{\boldsymbol{X}}_6^T \end{bmatrix} \begin{bmatrix} \widehat{\boldsymbol{x}}_1 & \cdots & \widehat{\boldsymbol{x}}_6 \end{bmatrix} = \begin{bmatrix} d_{11} & & \boldsymbol{0} \\ & \ddots & \\ \boldsymbol{0} & & d_{66} \end{bmatrix} \tag{22}$$

where $d_{ii} = \widehat{\boldsymbol{X}}_i^T\widehat{\boldsymbol{x}}_i$ ($\theta_{ii} = -\pi/2$ in (21)). Then, we can obtain $\boldsymbol{S}^{-1}$ as

$$\boldsymbol{S}^{-1} = \begin{bmatrix} d_{11}^{-1} & & \boldsymbol{0} \\ & \ddots & \\ \boldsymbol{0} & & d_{66}^{-1} \end{bmatrix} \boldsymbol{S}_r^T \tag{23}$$

Premultiplying right side of (13) by $\boldsymbol{S}^{-T}\boldsymbol{S}^T$ and substituting (11) and (23) into (13), $\boldsymbol{K}$ can be represented

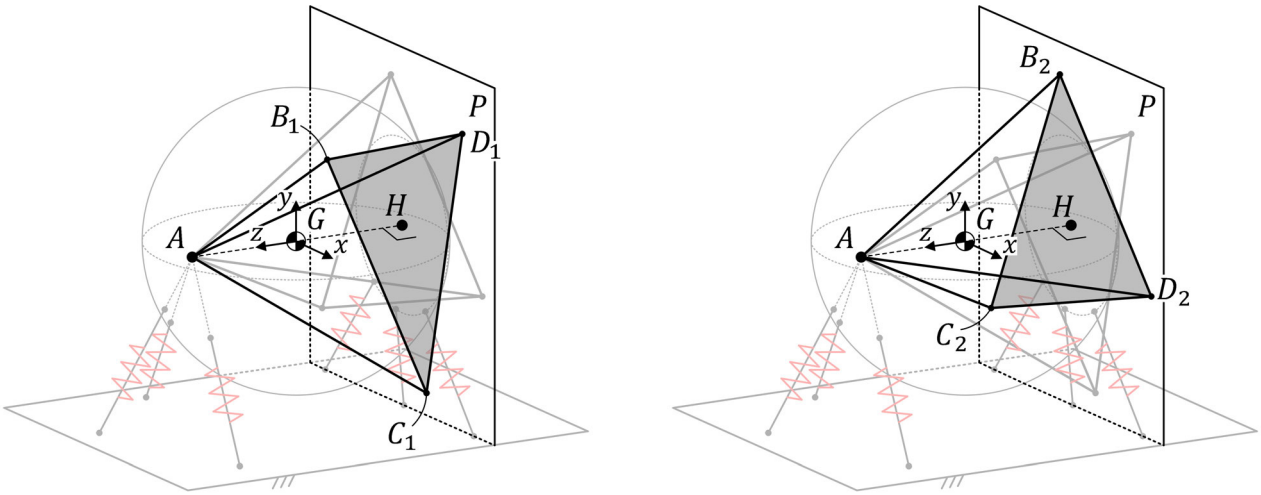

(a) (b)

FIGURE 8. Two orthocentric tetrahedral in a vibration system.

as

$$\boldsymbol{K} = \boldsymbol{S}_r \begin{bmatrix} \tilde{m}_1\omega_1^2 d_{11}^{-2} & & \boldsymbol{0} \\ & \ddots & \\ \boldsymbol{0} & & \tilde{m}_6\omega_6^2 d_{66}^{-2} \end{bmatrix} \boldsymbol{S}_r^T$$

and $\boldsymbol{K}$ is given in a similar form of (1)

$$\boldsymbol{K} = \sum_{i=1}^{3} \tilde{m}_i\omega_i^2 d_{ii}^{-2}\widehat{\boldsymbol{x}}_i\widehat{\boldsymbol{x}}_i^T + \sum_{i=4}^{6} \tilde{m}_i\omega_i^2 d_{ii}^{-2}\widehat{\boldsymbol{x}}_i\widehat{\boldsymbol{x}}_i^T. \quad (24)$$

Clearly, $\mathrm{tr}\,(\boldsymbol{K}\boldsymbol{\Delta}) = 0$ since $\widehat{\boldsymbol{x}}_i\boldsymbol{\Delta}\widehat{\boldsymbol{x}}_i^T = 0$ for all i. Therefore, if the modal matrix $\boldsymbol{S}$ is specified using the orthocentric tetrahedra, the stiffness matrix determined from (13) can always be realized by means of the parallel connection of line springs.

Additionally, the first and second terms of the right side of (24) correspond to $\boldsymbol{K}_2$ and $\boldsymbol{K}_1$ in (1), respectively, since $\widehat{\boldsymbol{x}}_i$'s (for $i = 1, 2, 3$) are the lines of action lying on the plane P and $\widehat{\boldsymbol{x}}_i$'s (for $i = 4, 5, 6$) are ones intersecting the point A (Fig. 4).

IV. DESIGN METHOD

A. DESIGN PARAMETERS

In this subsection, we consider the parameters that are used to determine two orthocentric tetrahedra. For the simplicity of design, the co-ordinate frame is chosen such that the origin coincides with the center of mass and we let the intersecting point A $(0, 0, z_1)$ lie on the z-axis and the plane $P(z = z_2)$ be perpendicular to the z-axis (Fig. 8). Since G is the internal division of $\overline{AH}$ and $\overline{AG}\cdot\overline{GH} = r_g^2$, z_1 and z_2 should satisfy the following relation:

$$z_1 z_2 = -r_g^2 \quad (25)$$

As shown in Fig. 8, we select six points (B_1, B_2, C_1, C_2, D_1, and D_2) on the plane $P(z = z_2)$ such that the two tetrahedra ($AB_1C_1D_1$ and $AB_2C_2D_2$) are orthocentric. It can be shown from (20) and (21) that even if one of the tetrahedra rotates about the z-axis, the vibration modes still satisfy orthogonality with respect to the mass matrix. Thus, we can assume that B_1 and B_2 lie on the zx- and yz-planes, respectively (Fig. 9). Then, the co-ordinates of the points can be written as B_1 $(x_2, 0, z_2)$ and B_2 $(0, Y_2, z_2)$. Since H is the orthocenter of the triangles ($B_1C_1D_1$ and $B_2C_2D_2$), $\overline{C_1D_1}$ and $\overline{C_2D_2}$ are respectively parallel to the y- and x-axes, and therefore their co-ordinates can be written as C_1 (x_3, y_3, z_2), D_1 (x_3, y_4, z_2), C_2 (X_3, Y_3, z_2) and D_2 (X_4, Y_3, z_2) as illustrated in Fig. 9.

Now, the vibration modes can be expressed in terms of the co-ordinates of the seven points. The unit direction and position vectors of $\widehat{\boldsymbol{X}}_1$ are given by $\boldsymbol{s}_1 = \overrightarrow{B_1A}/\left\|\overrightarrow{B_1A}\right\|$ and $\boldsymbol{r}_1 = \overrightarrow{GA}$. Similarly, we can calculate the other $\boldsymbol{s}_i$'s and $\boldsymbol{r}_i$'s using (10) to obtain

$$\widehat{\boldsymbol{X}}_1 = \frac{1}{\left\|\overrightarrow{B_1A}\right\|}\begin{Bmatrix} 0 \\ x_2z_1 \\ 0 \\ x_2 \\ 0 \\ -z_1+z_2 \end{Bmatrix},$$

$$\widehat{\boldsymbol{X}}_2 = \frac{1}{\left\|\overrightarrow{C_1A}\right\|}\begin{Bmatrix} -y_3z_1 \\ x_3z_1 \\ 0 \\ x_3 \\ y_3 \\ -z_1+z_2 \end{Bmatrix},$$

$$\widehat{\boldsymbol{X}}_3 = \frac{1}{\left\|\overrightarrow{D_1A}\right\|}\begin{Bmatrix} -y_4z_1 \\ x_3z_1 \\ 0 \\ x_3 \\ y_3 \\ -z_1+z_2 \end{Bmatrix},$$

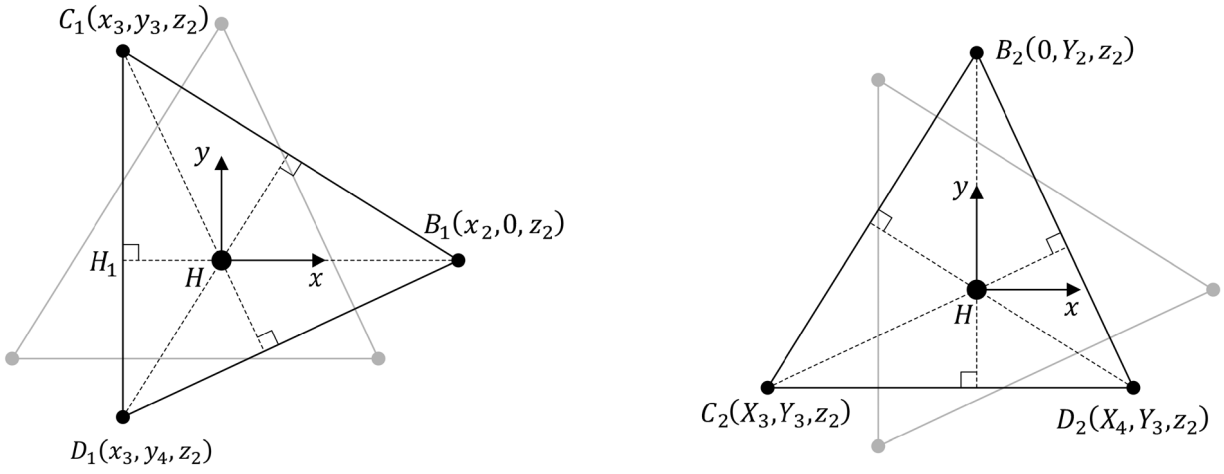

FIGURE 9. Six vertices on the plane P chosen to determine orthocentric tetrahedra.

$$\widehat{\boldsymbol{X}}_4 = \frac{1}{\left\|\overrightarrow{C_2D_2}\right\|}\begin{Bmatrix} 0 \\ z_2\,(X_4 - X_3) \\ -Y_3\,(X_4 - X_3) \\ X_4 - X_3 \\ 0 \\ 0 \end{Bmatrix},$$

$$\widehat{\boldsymbol{X}}_5 = \frac{1}{\left\|\overrightarrow{D_2B_2}\right\|}\begin{Bmatrix} -z_2\,(Y_2 - Y_3) \\ -z_2 X_4 \\ X_4 Y_2 \\ -X_4 \\ Y_2 - Y_3 \\ 0 \end{Bmatrix},$$

$$\widehat{\boldsymbol{X}}_6 = \frac{1}{\left\|\overrightarrow{B_2C_2}\right\|}\begin{Bmatrix} -z_2\,(Y_3 - Y_2) \\ z_2 X_3 \\ -X_3 Y_2 \\ X_3 \\ Y_3 - Y_2 \\ 0 \end{Bmatrix}. \tag{26}$$

If we let H_1 be the foot of perpendicular drawn from B_1 to $\overline{C_1D_1}$ (Fig. 9(a)), $\overline{GH_1}$ and the common normal to $\overline{C_1D_1}$ and $\overline{B_1A}$ are collinear. Thus, orthogonal relation $\overrightarrow{GH_1}\cdot\overrightarrow{B_1A} = 0$ gives:

$$-x_2x_3 = z_2^2 - z_1z_2 = z_2^2 + r_g^2, \tag{27a}$$

and $\overrightarrow{HC_1}\cdot\overrightarrow{D_1B_1} = 0$ (Fig. 9(a)) yields:

$$-y_3y_4 = x_3^2 - x_2x_3. \tag{27b}$$

In the similar manner, we can obtain the following relations between X_3, X_4, Y_2, and Y_3:

$$-X_3X_4 = Y_3^2 - Y_2Y_3, \tag{28a}$$

$$-Y_2Y_3 = z_2^2 + r_g^2. \tag{28b}$$

Because we have ten parameters (x_2, x_3, y_3, y_4, X_3, X_4, Y_2, Y_3, z_1, and z_2) in five equations (26), (27a), (27b), (28a), and (28b), there exist five free choices. In the design process, we will use the following five dimensionless variables to determine two orthocentric tetrahedra:

$$h = -\frac{z_2}{z_1},\quad u = -\frac{x_3}{x_2},\ v = -\frac{y_4}{y_3},$$
$$U = -\frac{Y_3}{Y_2},\quad V = -\frac{X_4}{X_3}. \tag{29}$$

Now, the ten parameters can be rewritten in terms of the dimensionless variables as

$$\begin{aligned}
z_1 &= r_g\frac{1}{\sqrt{h}},\quad z_2 = -r_g\sqrt{h},\\
x_2 &= r_g\sqrt{\frac{h+1}{u}},\quad x_3 = -r_g\sqrt{(h+1)\,u},\\
y_3 &= r_g\sqrt{\frac{(h+1)\,(u+1)}{v}},\\
y_4 &= -r_g\sqrt{(h+1)\,(u+1)\,v},\\
X_3 &= -r_g\sqrt{\frac{(h+1)\,(U+1)}{V}},\\
X_4 &= r_g\sqrt{(h+1)\,(U+1)\,V},\\
Y_2 &= r_g\sqrt{\frac{(h+1)}{U}},\quad Y_3 = -r_g\sqrt{(h+1)\,U}.
\end{aligned} \tag{30}$$

B. DESIGN OF A DIRECT EXCITATION SYSTEM

If an oscillatory force $\boldsymbol{F}_{ext}$ is externally applied to a rigid body supported by springs and dampers, the equation of motion is given by

$$\boldsymbol{M}\ddot{\boldsymbol{X}} + \boldsymbol{C}\dot{\boldsymbol{X}} + \boldsymbol{K}\boldsymbol{X} = \boldsymbol{F}_{ext}, \tag{31}$$

where $\boldsymbol{C}$ is the damping matrix. It is assumed that the damping matrix $\boldsymbol{C}$ can be diagonalized by the modal matrix $\boldsymbol{S}$ as

follows:

$$\boldsymbol{S}^T\boldsymbol{C}\boldsymbol{S} = \begin{bmatrix} \tilde{c}_1 & & \boldsymbol{0} \\ & \ddots & \\ \boldsymbol{0} & & \tilde{c}_6 \end{bmatrix}, \tag{32}$$

where $\tilde{c}_i = \widehat{\boldsymbol{X}}_i^T \boldsymbol{C}\widehat{\boldsymbol{X}}_i$. The applied force can be expressed as

$$\boldsymbol{F}_{ext} = f\widehat{\boldsymbol{s}}_f e^{i\Omega t}, \tag{33}$$

where f is the intensity of the force and Ω is the driving frequency. $\widehat{\boldsymbol{s}}_f$ is the line of action of the force

$$\widehat{\boldsymbol{s}}_f = \begin{Bmatrix} \boldsymbol{s}_f \\ \boldsymbol{r}_f \times \boldsymbol{s}_f \end{Bmatrix}. \tag{34}$$

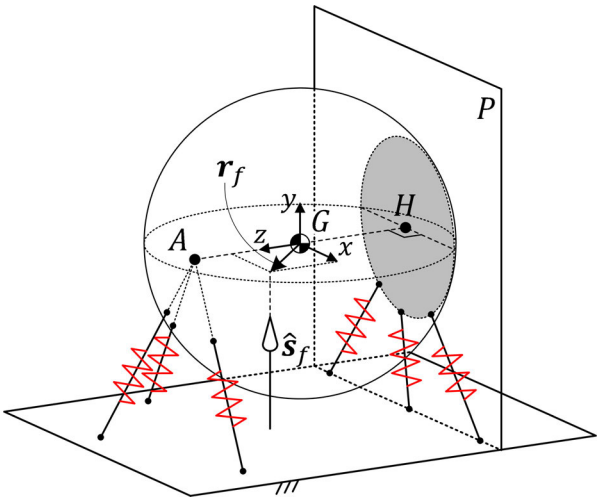

FIGURE 10. Direct excitation system.

If we choose the co-ordinate frame such that the y-axis is parallel to $\widehat{\boldsymbol{s}}_f$ (Fig. 10), the position vector can be selected as $\boldsymbol{r}_f = \begin{Bmatrix} r_x & 0 & r_z \end{Bmatrix}^T$, and the line of action $\widehat{\boldsymbol{s}}_f$ becomes:

$$\widehat{\boldsymbol{s}}_f = \begin{Bmatrix} 0 & 1 & 0 & -r_z & 0 & r_x \end{Bmatrix}^T. \tag{35}$$

The time invariant form of (31) is written as

$$\left(\boldsymbol{K} - \Omega^2\boldsymbol{M} + j\Omega\boldsymbol{C}\right)\widehat{\boldsymbol{X}} = f\widehat{\boldsymbol{s}}_f. \tag{36}$$

$\widehat{\boldsymbol{X}}$ can be represented by the linear combination of the modes

$$\widehat{\boldsymbol{X}} = \boldsymbol{S}\boldsymbol{v}, \tag{37}$$

where $\boldsymbol{v} = \begin{Bmatrix} v_1 & \cdots & v_6 \end{Bmatrix}^T \in R^{6\times 1}$ is a constant vector. Premultiplying (36) by $\boldsymbol{S}^T$ and substituting (37) into (36) yields:

$$\begin{bmatrix} \tilde{k}_1 - \Omega^2\tilde{m}_1 + j\Omega\tilde{c}_1 & & \boldsymbol{0} \\ & \ddots & \\ \boldsymbol{0} & & \tilde{k}_6 - \Omega^2\tilde{m}_6 + j\Omega\tilde{c}_6 \end{bmatrix}\boldsymbol{v} = \begin{bmatrix} f\widehat{\boldsymbol{X}}_1^T\widehat{\boldsymbol{s}}_f \\ \vdots \\ f\widehat{\boldsymbol{X}}_6^T\widehat{\boldsymbol{s}}_f \end{bmatrix}. \tag{38}$$

Equation (38) gives:

$$v_i = \frac{f\widehat{\boldsymbol{X}}_i^T\widehat{\boldsymbol{s}}_f}{\tilde{k}_i - \Omega^2\tilde{m}_i + j\Omega\tilde{c}_i}. \tag{39}$$

Using (39), the frequency response is given by

$$\widehat{\boldsymbol{X}} = \sum_{i=1}^{6} v_i\widehat{\boldsymbol{X}}_i = \sum_{i=1}^{6}\left(\frac{f\widehat{\boldsymbol{X}}_i^T\widehat{\boldsymbol{s}}_f}{\tilde{k}_i - \Omega^2\tilde{m}_i + j\Omega\tilde{c}_i}\right)\widehat{\boldsymbol{X}}_i. \tag{40}$$

If the damping is assumed to be light damping, i.e., $\zeta_i = \frac{\tilde{c}_i}{2\tilde{m}_i\omega_i} < 0.05$, the ith resonant frequency Ω_i is almost the same as the ith natural frequency ω_i, i.e., $\Omega_i \approx \omega_i$ [19]. Thus, the dominant term of (40) at the ith resonant frequency Ω_i can be expressed approximately as

$$\widehat{\boldsymbol{X}}(\Omega = \Omega_i) \approx \frac{f\widehat{\boldsymbol{X}}_i^T\widehat{\boldsymbol{s}}_f}{j\Omega_i\tilde{c}_i}\widehat{\boldsymbol{X}}_i = \frac{f\widehat{\boldsymbol{X}}_i^T\widehat{\boldsymbol{s}}_f}{j2\tilde{m}_i\Omega_i^2\zeta_i}\widehat{\boldsymbol{X}}_i. \tag{41}$$

In what follows, when the driving frequency matches the ith resonant frequency, the work done by external force during one cycle can be written as

$$W_i = \int_0^{\frac{2\pi}{\Omega_i}} \mathrm{Re}\left[\boldsymbol{F}_{ext}\right]\cdot\mathrm{Re}\left[\dot{\boldsymbol{X}}\right]dt, \tag{42}$$

where $\mathrm{Re}\left[\boldsymbol{F}_{ext}\right]\cdot\mathrm{Re}\left[\dot{\boldsymbol{X}}\right]$ represents the instantaneous power. From (41), $\dot{X}$ is given by

$$\dot{\boldsymbol{X}} = j\Omega_i\widehat{\boldsymbol{X}}_i e^{j\Omega_i t} = \frac{f\widehat{\boldsymbol{X}}_i^T\widehat{\boldsymbol{s}}_f}{2\tilde{m}_i\Omega_i\zeta_i}\widehat{\boldsymbol{X}}_i e^{j\Omega_i t}. \tag{43}$$

Thus, the work is given by

$$W_i = \int_0^{\frac{2\pi}{\Omega_i}} \frac{f^2\left(\widehat{\boldsymbol{X}}_i^T\widehat{\boldsymbol{s}}_f\right)^2}{2\tilde{m}_i\Omega_i\zeta_i}\cos^2\Omega_i t\,dt.$$

or,

$$W_i = \frac{\pi f^2\left(\widehat{\boldsymbol{X}}_i^T\widehat{\boldsymbol{s}}_f\right)^2}{2\tilde{m}_i\Omega_i^2\zeta_i} = \frac{\pi f^2}{2\Omega_i^2\zeta_i}\cdot\frac{\left(\widehat{\boldsymbol{X}}_i^T\widehat{\boldsymbol{s}}_f\right)^2}{\widehat{\boldsymbol{X}}_i^T\boldsymbol{M}\widehat{\boldsymbol{X}}_i}. \tag{44}$$

If we substitute (14), (26), and (35) into (44) and summarize using (25), (27), and (28), we can obtain:

$$W_1 = \varepsilon_1\cdot\frac{\left\{r_x\left(z_2^2 + r_g^2\right) - \left(r_z z_2 + r_g^2\right)x_2\right\}^2}{r_g^2\left(z_2^2 + r_g^2\right)\left(x_2^2 + z_2^2 + r_g^2\right)},$$

$$W_2 = \varepsilon_2\cdot\frac{\left\{r_x\left(z_2^2 + r_g^2\right) - \left(r_z z_2 + r_g^2\right)x_3\right\}^2}{r_g^2\left(z_2^2 + r_g^2\right)\left(x_3^2 + y_3^2 + z_2^2 + r_g^2\right)},$$

$$W_3 = \varepsilon_3\cdot\frac{\left\{r_x\left(z_2^2 + r_g^2\right) - \left(r_z z_2 + r_g^2\right)x_3\right\}^2}{r_g^2\left(z_2^2 + r_g^2\right)\left(x_3^2 + y_4^2 + z_2^2 + r_g^2\right)},$$

$$W_4 = \varepsilon_4\cdot\frac{Y_2^2\left(z_2 - r_z\right)^2}{\left(z_2^2 + r_g^2\right)\left(Y_2^2 + z_2^2 + r_g^2\right)},$$

$$W_5 = \varepsilon_5 \cdot \frac{Y_3^2 (z_2 - r_z)^2}{\left(z_2^2 + r_g^2\right)\left(X_3^2 + Y_3^2 + z_2^2 + r_g^2\right)},$$
$$W_6 = \varepsilon_6 \cdot \frac{Y_3^2 (z_2 - r_z)^2}{\left(z_2^2 + r_g^2\right)\left(X_4^2 + Y_3^2 + z_2^2 + r_g^2\right)}, \quad (45)$$

where $\varepsilon_i = \frac{\pi f^2}{2m\zeta_i\Omega_i^2}$. Substituting (30) into (45) yields:

$$W_1 = \varepsilon_1 \cdot \frac{\left\{p_x\sqrt{(h+1)\,u} - \left(1 - p_z\sqrt{h}\right)\right\}^2}{(h+1)\,(u+1)}, \quad (46a)$$
$$W_2 = \varepsilon_2 \cdot \frac{v\left\{\left(1 - p_z\sqrt{h}\right)\sqrt{u} + p_x\sqrt{h+1}\right\}^2}{(h+1)\,(u+1)\,(v+1)}, \quad (46b)$$
$$W_3 = \varepsilon_3 \cdot \frac{\left\{\left(1 - p_z\sqrt{h}\right)\sqrt{u} + p_x\sqrt{h+1}\right\}^2}{(h+1)\,(u+1)\,(v+1)}, \quad (46c)$$
$$W_4 = \varepsilon_4 \cdot \frac{\left(\sqrt{h} + p_z\right)^2}{(h+1)\,(U+1)}, \quad (47a)$$
$$W_5 = \varepsilon_5 \cdot \frac{UV\left(\sqrt{h} + p_z\right)^2}{(h+1)\,(U+1)\,(V+1)}, \quad (47b)$$
$$W_6 = \varepsilon_6 \cdot \frac{U\left(\sqrt{h} + p_z\right)^2}{(h+1)\,(U+1)\,(V+1)}, \quad (47c)$$

where $p_x = r_x/r_g$ and $p_z = r_z/r_g$.

For the given m, Ω_i's, ζ_i's, p_x, and p_z, if the desired ratios are prescribed as $\gamma_i = W_{i+1}/W_1$ $(i = 1, \ldots, 5)$, we can get the five equations, and thereby we may obtain the finite number of solutions of h, u, v, U, and V. From (46b), (46c), (47b), and (47c), v and V are determined as

$$v = \frac{\gamma_1\zeta_2\Omega_2^2}{\gamma_2\zeta_3\Omega_3^2} \quad (48)$$

and

$$V = \frac{\gamma_4\zeta_5\Omega_5^2}{\gamma_5\zeta_6\Omega_6^2}. \quad (49)$$

From (47) and (49), we can determine U as

$$U = \frac{\gamma_4\zeta_5\Omega_5^2 + \gamma_5\zeta_6\Omega_6^2}{\gamma_3\zeta_4\Omega_4^2}. \quad (50)$$

Using (46) and (48), $\sqrt{u}$ can be expressed in terms of h as

$$\sqrt{u} = \frac{\pm R_1\left(1 - p_z\sqrt{h}\right) - p_x\sqrt{h+1}}{\left(1 - p_z\sqrt{h}\right) \pm R_1 p_x\sqrt{h+1}}, \quad (51)$$

where $R_1 = \sqrt{\frac{\gamma_1\zeta_2\Omega_2^2 + \gamma_2\zeta_3\Omega_3^2}{\zeta_1\Omega_1^2}}$. Substituting (50) and (51) into (46d) and (46a), respectively, and dividing (46d) by (46a) yields the quadratic equation in terms of $\sqrt{h}$:

$$\left(p_x^2 + p_z^2 - R_2^2\right)\left(\sqrt{h}\right)^2 - 2p_z\left(R_2^2 + 1\right)\sqrt{h} + p_x^2 - R_2^2 p_z^2 + 1 = 0, \quad (52)$$

where $R_2 = \sqrt{\frac{\zeta_1\Omega_1^2 + \gamma_1\zeta_2\Omega_2^2 + \gamma_2\zeta_3\Omega_3^2}{\gamma_3\zeta_4\Omega_4^2 + \gamma_4\zeta_5\Omega_5^2 + \gamma_5\zeta_6\Omega_6^2}}$. For $p_x^2 + p_z^2 - R_2^2 \neq 0$, the solutions of (52) are given by

$$\sqrt{h} = \frac{p_z\left(R_2^2 + 1\right) \pm \sqrt{D}}{p_x^2 + p_z^2 - R_2^2}, \quad (53)$$

where $D = -\left(p_x^2 + p_z^2 + 1\right)\left(p_x^2 - R_2^2 p_z^2 - R_2^2\right)$. If $p_x^2 + p_z^2 - R_2^2 = 0$, $\sqrt{h}$ becomes:

$$\sqrt{h} = \frac{1 - p_z^2}{2p_z}. \quad (54)$$

Close observations on (52), (53), and (54) reveal the following findings:

1) When $p_x^2 + p_z^2 - R_2^2 \neq 0$, (52) has a real root if and only if $(p_x, p_z) \in \left\{(p_x, p_z)\,|\,\frac{p_x^2}{R_2^2} - p_z^2 \leq 1\right\}$.
2) For (p_x, p_z) such that $\frac{p_x^2}{R_2^2} - p_z^2 \leq 1$ and $p_x^2 + p_z^2 - R_2^2 \neq 0$, if the sum of the roots of (52) is positive or their product is negative, i.e., $(p_x, p_z) \in \left\{(p_x, p_z)\,|\,\frac{2p_z(R_2^2+1)}{p_x^2+p_z^2-R_2^2} > 0 \text{ or } \frac{p_x^2 - R_2^2 p_z^2 + 1}{p_x^2+p_z^2-R_2^2} < 0\right\}$, then there exists at least one solution such that $\sqrt{h} > 0$.
3) When $p_x^2 + p_z^2 - R_2^2 = 0$, $p_z \in \{p_z | p_z < -1 \text{ or } 0 < p_z < 1\}$ since $\sqrt{h} > 0$.

From these findings, we can obtain the feasible region of the points (p_x, p_z) (Fig. 11). Therefore, it can be said that the existence of a positive root of (52) depends on R_2 and the position vector $\boldsymbol{r}_f = \{r_x\ 0\ r_z\}^T$.

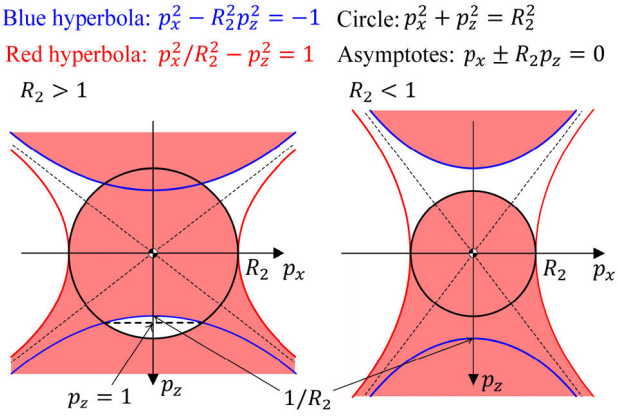

FIGURE 11. Feasible region (red region) of the points (p_x, p_z) such that there exists a positive solution of $\sqrt{h}$.

Finally, from (51) and (53) (or (54)), we can acquire the solutions of $\sqrt{u}$. Theoretically, the maximum number of $\sqrt{u}$ is four, if there is a positive value of $\sqrt{u}$, we choose one of them, then two tetrahedral (or modal matrix $\boldsymbol{S}$) can be determined for a vibrating system to satisfy the requirement.

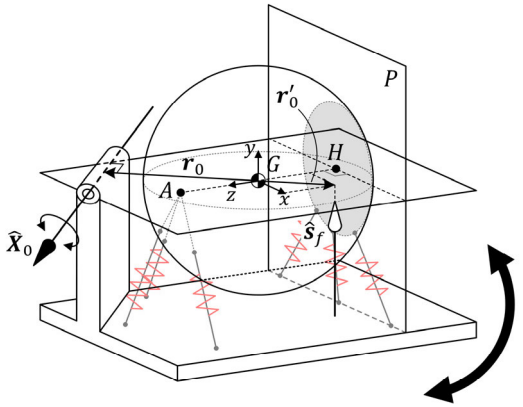

FIGURE 12. Base excitation system.

C. DESIGN OF BASE EXCITATION SYSTEM

The equation of motion for a base-excited system can be written as (Fig. 12)

$$\boldsymbol{M}\ddot{\boldsymbol{Z}} + \boldsymbol{C}\dot{\boldsymbol{Z}} + \boldsymbol{K}\boldsymbol{Z} = -\boldsymbol{M}\ddot{\boldsymbol{X}}_0, \tag{55}$$

where $\boldsymbol{X}_0$ is a small displacement of foundation and $\boldsymbol{Z}(=\boldsymbol{X}-\boldsymbol{X}_0)$ is the relative displacement of the rigid body with respect to the foundation. The time invariant form of (55) is

$$\left(-\Omega^2\boldsymbol{M} + j\Omega\boldsymbol{C} + \boldsymbol{K}\right)\widehat{\boldsymbol{Z}} = \Omega^2\boldsymbol{M}\widehat{\boldsymbol{X}}_0\left(=\widehat{\boldsymbol{F}}_{ext}\right). \tag{56}$$

If the base is harmonically rotated about the axis, then $\widehat{\boldsymbol{X}}_0$ can be written in terms of a line vector

$$\widehat{\boldsymbol{X}}_0 = \phi_0 \begin{Bmatrix} \boldsymbol{r}_0 \times \boldsymbol{s}_0 \\ \boldsymbol{s}_0 \end{Bmatrix},$$

where ϕ_0 is the amplitude of oscillatory rotation. The external force $\widehat{\boldsymbol{F}}_{ext}$ in (56) can be expressed in terms of a line of action $\widehat{\boldsymbol{s}}_f$

$$\widehat{\boldsymbol{F}}_{ext} = f_B\widehat{\boldsymbol{s}}_f = mr_0\phi_0\Omega^2 \begin{Bmatrix} \boldsymbol{s}'_0 \\ \boldsymbol{r}'_0 \times \boldsymbol{s}'_0 \end{Bmatrix}, \tag{57}$$

where $\boldsymbol{s}'_0 = \frac{\boldsymbol{r}_0 \times \boldsymbol{s}_0}{r_0}$, $\boldsymbol{r}'_0 = -\left(\frac{r_g}{r_0}\right)^2 \boldsymbol{r}_0$, $r_0 = \|\boldsymbol{r}_0\|$, and $\boldsymbol{r}_0 \perp \boldsymbol{s}_0$. Although the intensity of the force $f_B\left(=mr_0\phi_0\Omega^2\right)$ seems to be proportional to Ω^2, we consider f_B to be constant throughout the driving frequency since the input acceleration due to base excitation is assumed to stay the same in a practical design of a base excitation system.

If the co-ordinate frame is selected such that the rotation axis of the foundation lies on the zx-plane, $\boldsymbol{s}'_0$ and $\boldsymbol{r}'_0$ can be given by $\boldsymbol{s}'_0 = \left\{0\ 1\ 0\right\}^T$ and $\boldsymbol{r}'_0 = \left\{r'_{0x}\ 0\ r'_{0z}\right\}^T$. The external force becomes parallel to the y-axis

$$\widehat{\boldsymbol{F}}_{ext} = f_B\left\{0 \quad 1 \quad 0 \quad -r'_{0z} \quad 0 \quad r'_{0x}\right\}^T. \tag{58}$$

The energy produced by the relative vibration caused by base excitation at $\Omega = \Omega_i$ during one cycle is

$$W_i = \int_0^{\frac{2\pi}{\Omega_i}} \mathrm{Re}\left[\boldsymbol{F}_{ext}\right] \cdot \mathrm{Re}\left[\dot{Z}\right] dt,$$

where

$$\dot{Z} = \frac{f\widehat{\boldsymbol{X}}_i^T\widehat{\boldsymbol{s}}_f}{2\tilde{m}_i\Omega_i\zeta_i}\widehat{\boldsymbol{X}}_i e^{j\Omega_i t}.$$

Accordingly, W_i can be obtained by substituting $f = f_B$, $p_x = r'_{0x}/r_g$, and $p_z = r'_{0z}/r_g$ into (46), and thus we can directly use the aforementioned solutions of the direct excitation system to obtain two orthocentric tetrahedra such that a base excitation system has the prespecified ratio of energy peaks.

If the vibration axis $\widehat{\boldsymbol{X}}_0$ goes to infinity, the input displacement of base excitation becomes a repetitive translational motion

$$\widehat{\boldsymbol{X}}_0 = \delta_0\left\{0 \quad 1 \quad 0 \quad 0 \quad 0 \quad 0\right\}^T.$$

where δ_0 is the amplitude of translational vibration. In this case, the direction of translation becomes parallel to the y-axis of the co-ordinate frame. The external force in (58) becomes:

$$\widehat{\boldsymbol{F}}_{ext} = f_B\left\{0 \quad 1 \quad 0 \quad 0 \quad 0 \quad 0\right\}^T,$$

where $f_B = m\delta_0\Omega^2$. Since $p_x = p_z = 0$ in (51) and (52), u and h are determined as

$$u = \frac{\gamma_1\zeta_2\Omega_2^2 + \gamma_2\zeta_3\Omega_3^2}{\zeta_1\Omega_1^2} \tag{59}$$

and

$$h = \frac{\gamma_3\zeta_4\Omega_4^2 + \gamma_4\zeta_5\Omega_5^2 + \gamma_5\zeta_6\Omega_6^2}{\zeta_1\Omega_1^2 + \gamma_1\zeta_2\Omega_2^2 + \gamma_2\zeta_3\Omega_3^2}. \tag{60}$$

Since v, V, and U are independent of p_x and p_z, they are given by $v = \frac{\gamma_1\zeta_2\Omega_2^2}{\gamma_2\zeta_3\Omega_3^2}$, $V = \frac{\gamma_4\zeta_5\Omega_5^2}{\gamma_5\zeta_6\Omega_6^2}$, and $U = \frac{\gamma_4\zeta_5\Omega_5^2 + \gamma_5\zeta_6\Omega_6^2}{\gamma_3\zeta_4\Omega_4^2}$.

V. NUMERICAL EXAMPLES

In this section, we present a design example of a vibration energy harvester to demonstrate how to utilize the proposed design method. It will be shown that the method can be used to widen the valid working bandwidth within a target frequency range.

In order to illustrate the design process and advantages of the proposed design method, four spatial vibration systems under base excitation (energy harvesters) are designed. We assume 1) that mass properties in all the systems are given by $m = 0.04$ kg and $I = 1.6 \times 10^{-6}$ kg·m^2, 2) that the base excitation is a repetitive translational motion such that f_B of 1.5 N is constant throughout the driving frequency, and 3) that all the modal damping ratios are identical, i.e., $\zeta_1 = \zeta_2 = \cdots = \zeta_6 = \zeta$. The reference frame $G - xyz$ is chosen such that its origin is positioned at the mass center and the y-axis is parallel to the translational motion of base (Fig. 13). The design requirement is that the range of the bandwidth is from 50 Hz to 75 Hz. To achieve

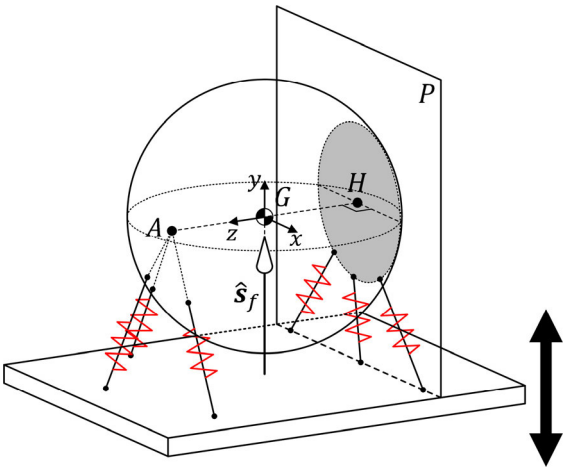

FIGURE 13. Vibration system embedded on the foundation that vibrates translationally.

this, we specify the desired resonance frequencies as follows:

$$\Omega_1 = 50 \text{ Hz}, \quad \Omega_2 = 60 \text{ Hz}, \Omega_3 = 70 \text{ Hz},$$
$$\Omega_4 = 55 \text{ Hz}, \Omega_5 = 65 \text{ Hz}, \quad \text{and } \Omega_6 = 75 \text{ Hz}. \tag{61}$$

For each system, we set the work ratios as follows:

1) *System*1 : $1 : \gamma_1 : \gamma_2 : \gamma_3 : \gamma_4 : \gamma_5 = 1 : 1 : 1 : 1 : 1 : 1$

2) *System*2 : $1 : \gamma_1 : \gamma_2 : \gamma_3 : \gamma_4 : \gamma_5 = 1 : 1 : 0.5 : 1 : 0.5 : 0.5$

3) *System*3 : $1 : \gamma_1 : \gamma_2 : \gamma_3 : \gamma_4 : \gamma_5 = 1 : 1 : 1 : 2 : 2 : 2$

4) *System*4 : $1 : \gamma_1 : \gamma_2 : \gamma_3 : \gamma_4 : \gamma_5$
$= 1 : 1.8 : 2.6 : 1.4 : 2.2 : 3.$ (62)

The frequency responses will be plotted for all systems (Fig. 15), but the design process is described in detail for only the case of *System 1*.

On the assumption of the identical modal damping ratio, substituting (61) and (62) into (47), (49), (50), (59), and (60), the dimensionless variables are determined as

$$h = 1.1705, \quad u = 3.400, \ v = 0.7347,$$
$$U = 3.2562, \quad V = 0.7511. \tag{63}$$

Using (30), the co-ordinates x_2, x_3, y_3, y_4, X_3, X_4, Y_2, Y_3, z_1, and z_2 can be computed as

$$x_2 = 0.0051, \quad x_3 = -0.0172,$$
$$y_3 = 0.0228, \quad y_4 = -0.0168,$$
$$X_3 = -0.0222, \quad X_4 = 0.0167,$$
$$Y_2 = 0.0052, \quad Y_3 = -0.0168,$$
$$z_1 = 0.0058, \quad \text{and } z_2 = -0.0068 \text{ (m)} \tag{64}$$

The two orthocentric tetrahedra are shown in Fig. 14. The vibration modes $\widehat{\boldsymbol{X}}_i$'s are calculated from (26) as

$$\widehat{\boldsymbol{X}}_1 = \begin{bmatrix} 0 \\ -0.0022 \\ 0 \\ -0.3700 \\ 0 \\ 0.9290 \end{bmatrix}, \quad \widehat{\boldsymbol{X}}_2 = \begin{bmatrix} 0.0043 \\ 0.0032 \\ 0 \\ 0.5499 \\ -0.7298 \\ 0.4061 \end{bmatrix},$$
$$\widehat{\boldsymbol{X}}_3 = \begin{bmatrix} -0.0036 \\ 0.0037 \\ 0 \\ 0.6329 \\ 0.6172 \\ 0.4674 \end{bmatrix},$$
$$\widehat{\boldsymbol{X}}_4 = \begin{bmatrix} 0 \\ -0.0068 \\ 0.0168 \\ 1 \\ 0 \\ 0 \end{bmatrix}, \quad \widehat{\boldsymbol{X}}_5 = \begin{bmatrix} 0.0055 \\ 0.0041 \\ 0.0031 \\ -0.6041 \\ 0.7969 \\ 0 \end{bmatrix},$$
$$\widehat{\boldsymbol{X}}_6 = \begin{bmatrix} -0.0048 \\ 0.0049 \\ 0.0037 \\ -0.7103 \\ -0.7038 \\ 0 \end{bmatrix},$$

and the lines of action $\widehat{\boldsymbol{x}}_i$'s from (16) as

$$\widehat{\boldsymbol{x}}_1 = \begin{bmatrix} 0 \\ -1 \\ 0 \\ -0.0068 \\ 0 \\ 0.0172 \end{bmatrix}, \quad \widehat{\boldsymbol{x}}_2 = \begin{bmatrix} 0.7987 \\ 0.6018 \\ 0 \\ 0.0041 \\ -0.0055 \\ 0.0030 \end{bmatrix},$$
$$\widehat{\boldsymbol{x}}_3 = \begin{bmatrix} -0.6981 \\ 0.7160 \\ 0 \\ 0.0049 \\ 0.0048 \\ 0.0036 \end{bmatrix},$$
$$\widehat{\boldsymbol{x}}_4 = \begin{bmatrix} 0 \\ -0.3769 \\ 0.9262 \\ 0.0022 \\ 0 \\ 0 \end{bmatrix}, \quad \widehat{\boldsymbol{x}}_5 = \begin{bmatrix} 0.7251 \\ 0.5497 \\ 0.4148 \\ -0.0032 \\ 0.0042 \\ 0 \end{bmatrix},$$
$$\widehat{\boldsymbol{x}}_6 = \begin{bmatrix} -0.6203 \\ 0.6261 \\ 0.4725 \\ -0.0037 \\ -0.0036 \\ 0 \end{bmatrix}.$$

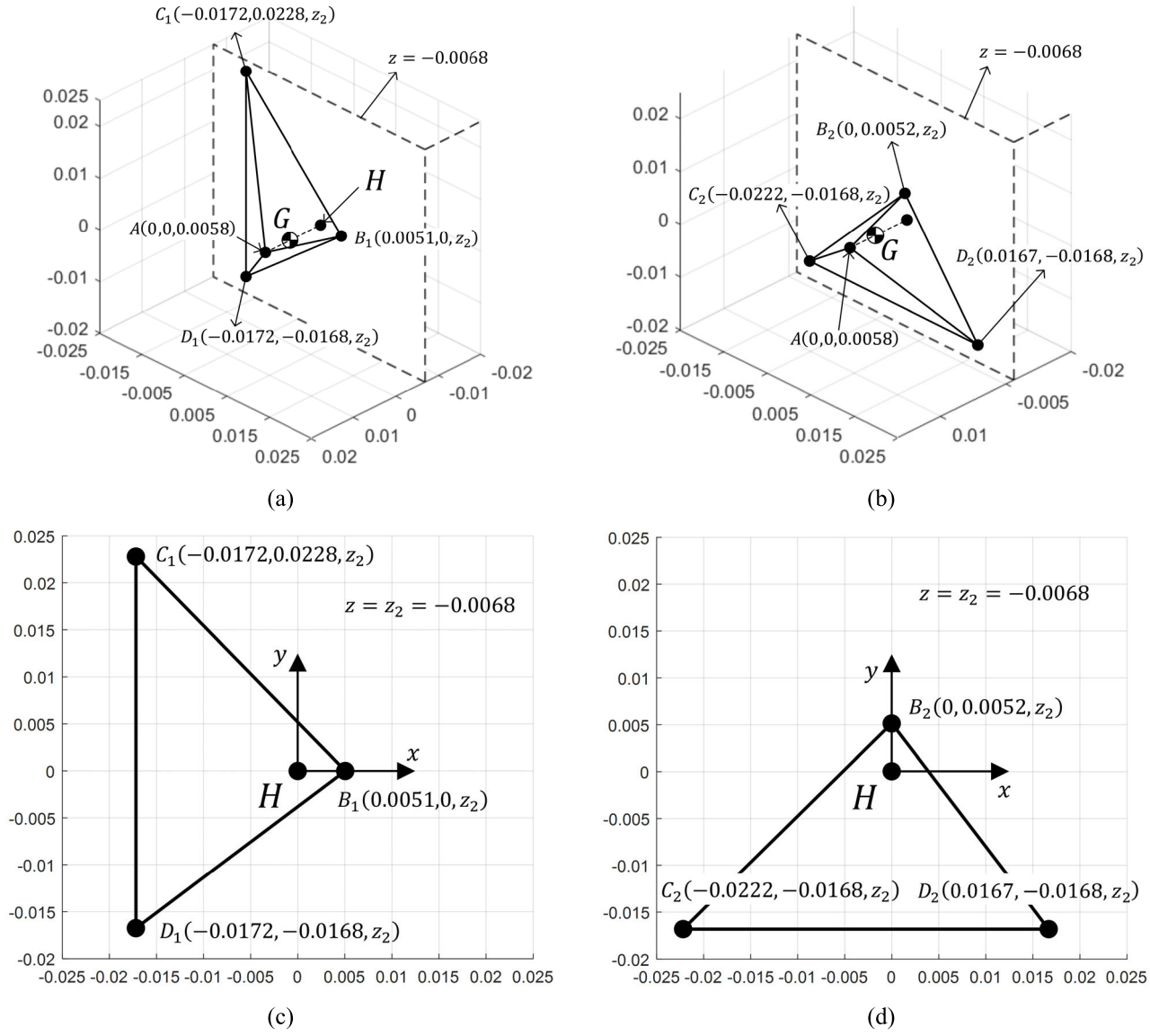

FIGURE 14. (a), (b) Synthesized orthocentric tetrahedra, (c) and (d) six vertices on the plane P.

Finally, the stiffness matrix $\boldsymbol{K}$ can be computed from (13) as

$$\boldsymbol{K}=\begin{bmatrix} 7129.1 & -926.9 & -389.5 & 0.2061 & 3.3599 & -2.0760 \\ & 6737.3 & 983.0 & -3.1145 & -0.2061 & 5.2541 \\ symm. & & 5518.7 & -5.7468 & -2.2768 & 0 \\ & & & 0.2664 & 0.0369 & 0.0360 \\ & symm. & & & 0.2818 & 0.0142 \\ & & & symm. & & 0.1845 \end{bmatrix}.$$

Using (24), the stiffness matrix can be separated into the sum of $\boldsymbol{K}_1$ and $\boldsymbol{K}_2$

$$\boldsymbol{K}_1=\begin{bmatrix} 4109.3 & -516.1 & -389.5 & 3.0171 & 24.0026 & 0 \\ & 3878.7 & 983.0 & -22.6745 & -3.0171 & 0 \\ symm. & & 5518.7 & -5.7468 & -2.2768 & 0 \\ & & & 0.1326 & 0.0176 & 0 \\ & symm. & & & 0.1404 & 0 \\ & & & symm. & & 0 \end{bmatrix},$$

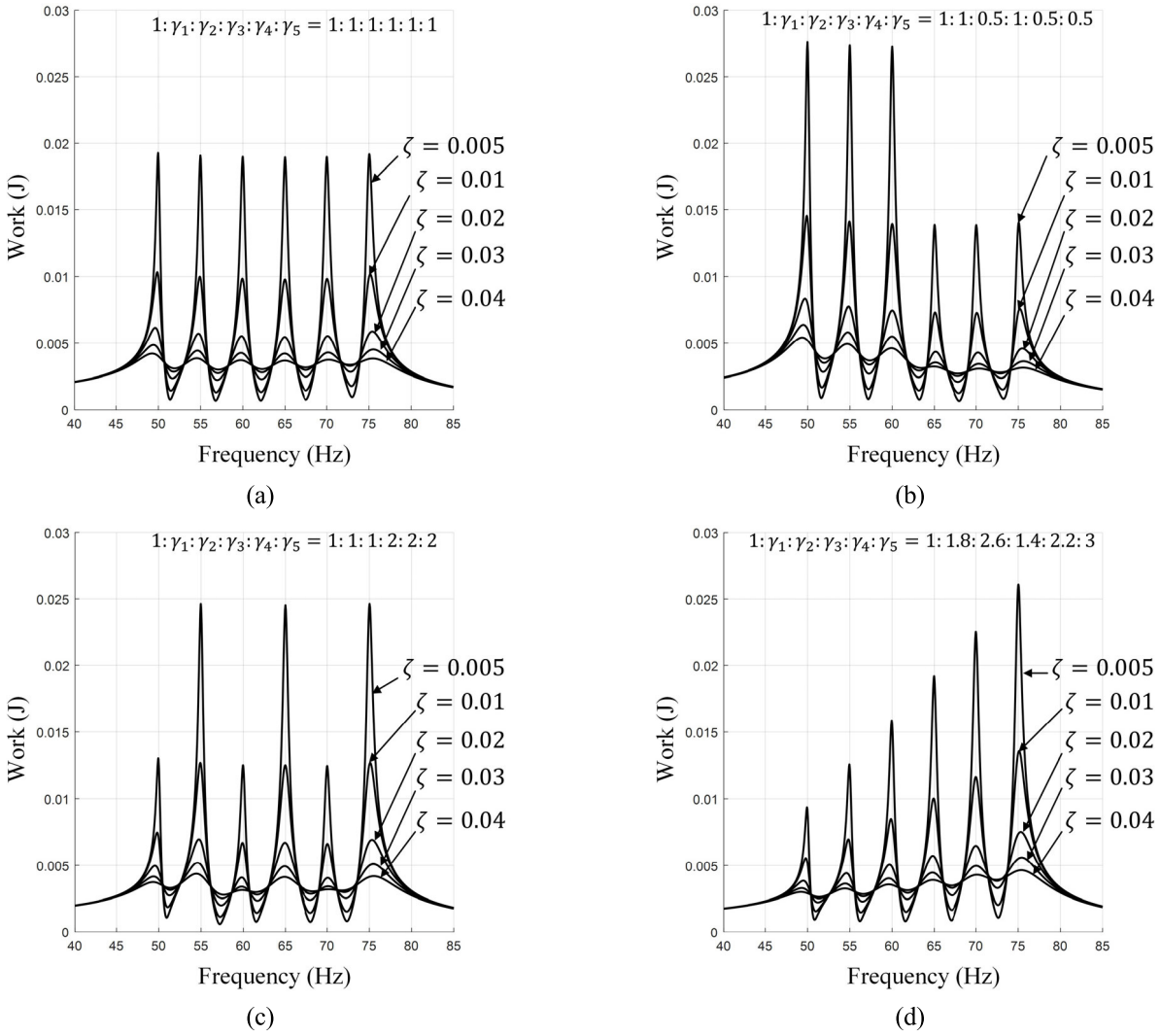

FIGURE 15. Frequency responses for various work ratios and damping ratios.

$$\boldsymbol{K}_2 = \begin{bmatrix} 3019.8 & -410.8 & 0 \\ & 2858.7 & 0 \\ \textit{symm.} & & 0 \\ & & \\ & \textit{symm.} & \end{bmatrix}$$

$$\begin{bmatrix} -2.8110 & -20.6626 & -2.0760 \\ 19.5600 & 2.8110 & 5.2541 \\ 0 & 0 & 0 \\ 0.1338 & 0.0192 & 0.0360 \\ & 0.1414 & 0.0142 \\ \textit{symm.} & & 0.1845 \end{bmatrix}.$$

Since $\mathrm{tr}\,(\boldsymbol{K}_1\boldsymbol{\Delta}) = \mathrm{tr}\,(\boldsymbol{K}_2\boldsymbol{\Delta}) = 0$, $\boldsymbol{K}_1$ and $\boldsymbol{K}_2$ can be realized by means of parallel connection of line springs. Using the realization technique proposed in [20], we can find one feasible set of six line springs. The lines of action of the springs are determined as

$$\widehat{\boldsymbol{\alpha}}_1 = \begin{bmatrix} 0 \\ -0.6428 \\ 0.7660 \\ 0.0038 \\ 0 \\ 0 \end{bmatrix}, \quad \widehat{\boldsymbol{\alpha}}_2 = \begin{bmatrix} -0.8467 \\ 0.3629 \\ 0.3891 \\ -0.0021 \\ -0.0049 \\ 0 \end{bmatrix},$$

$$\widehat{\boldsymbol{\alpha}}_3 = \begin{bmatrix} 0.3449 \\ 0.5902 \\ 0.7299 \\ -0.0035 \\ 0.0020 \\ 0 \end{bmatrix},$$

TABLE 1. Simulated values of energy peaks and work ratios for each damping ratio of system 1.

ζ	Simulated values of energy peaks (J)						Work ratio
	W_1	W_2	W_3	W_4	W_5	W_6	
0.005	0.01927	0.01908	0.01899	0.01896	0.01898	0.01918	1.0: 0.9899: 0.9855: 0.9863: 0.9848: 0.9953
0.01	0.01033	0.00999	0.00985	0.00979	0.00983	0.01016	1.0: 0.9674: 0.9533: 0.9497: 0.9518: 0.9836
0.02	0.00617	0.00573	0.00554	0.00547	0.00554	0.00589	1.0: 0.9275: 0.8969: 0.8864: 0.8980: 0.9545
0.03	0.00487	0.00444	0.00427	0.00422	0.0043	0.00453	1.0: 0.9121: 0.8766: 0.8672: 0.8831: 0.9293
0.04	0.00422	0.00386	0.00372	0.00369	0.00376	0.00384	1.0: 0.9156: 0.8831: 0.8745: 0.8903: 0.9106

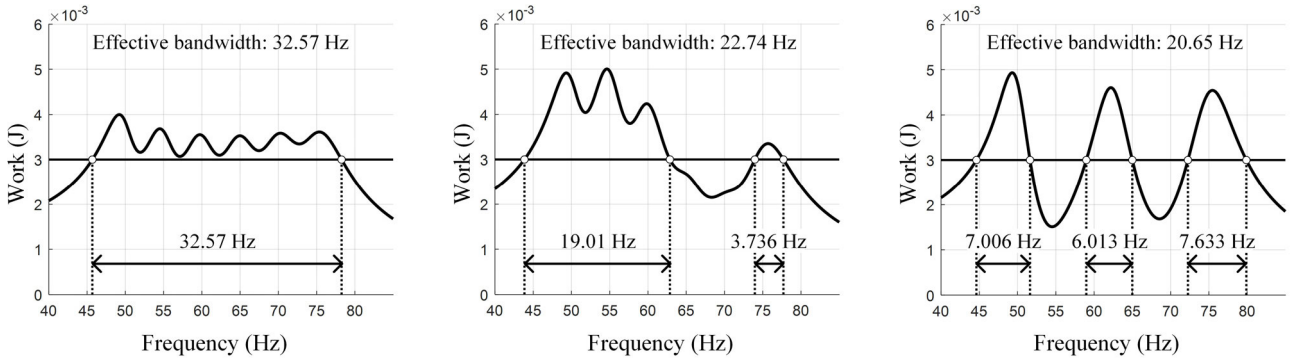

FIGURE 16. Frequency responses for (a) the specified work ratio of the 6-DOF spatial system, (b) arbitrary work ratio of the 6-DOF spatial system, and (c) the specified work ratio of the 3-DOF planar system.

$$\widehat{\boldsymbol{\beta}}_1 = \begin{bmatrix} -0.3420 \\ 0.9397 \\ 0 \\ 0.0064 \\ 0.0023 \\ -0.0051 \end{bmatrix}, \quad \widehat{\boldsymbol{\beta}}_2 = \begin{bmatrix} 0.8318 \\ -0.5550 \\ 0 \\ -0.0038 \\ -0.0057 \\ -0.0073 \end{bmatrix},$$

$$\widehat{\boldsymbol{\beta}}_3 = \begin{bmatrix} 0.8074 \\ 0.5900 \\ 0 \\ 0.0040 \\ -0.0055 \\ 0.0040 \end{bmatrix}.$$

and the spring constants are found:

$$k_{\alpha 1} = 3.6943, \quad k_{\alpha 2} = 4.9203, \quad k_{\alpha 3} = 4.8921,$$
$$k_{\beta 1} = 1.6688, \quad k_{\beta 2} = 2.0039, \quad k_{\beta 3} = 2.2057 (\times 10^3 \text{ N/m}).$$

The works generated by the base excitation are simulated for different work ratios and damping ratios (Fig. 15). The simulated values of energy peaks and their work ratios for each damping ratio of *System 1* are listed in Table 1.

Figure 16 illustrates the frequency responses of three different systems. Figure 16(a) depicts the frequency response of the spatial vibration system with the work ratio of 1 : 1 : 1 : 1 : 1 : 1 at the six target frequencies of (61). Figure 16(b) illustrates the frequency response of a spatial system designed for the target frequencies of (61) without consideration for work ratio. Figure 16(c) shows the frequency response of a planar system with work ratio of 1 : 1 : 1 at three target frequencies (50 Hz, 62.5 Hz, and 75 Hz). The design method of the planar system is explained in detail in [1]. For the three systems, the mass properties are identical and the identical damping ratio of $\zeta = 0.045$ is used.

For the effective bandwidths with the energy more than 0.003 J, Fig. 16 shows that the bandwidth illustrated in Fig. 16(a) is 57.7 % and 43.2 % wider than those shown in Fig. 16(b) and (c), respectively. In addition, the produced works at the valleys of the spatial system designed for specified work ratio are significantly greater than those of the other systems. Considering that energy produced by a typical vibration energy harvester is significantly reduced due to a slight deviation of the driving frequency from resonant frequencies, the high energy productions at the valleys are useful for designing a vibration energy harvester which requires a broad bandwidth. Therefore, the proposed method can be utilized to design a vibration energy harvester with a broad bandwidth.

VI. CONCLUSION

A novel method to design a spatial vibration system for prescribed work ratios at six target resonant frequencies is presented. This research makes two major contributions. First, the synthesis method of a spatial vibration system with a realizable stiffness matrix is developed through geometrical investigation into vibration modes. It is shown that six vibration axes and six lines of action obtained by transforming the vibration modes by the mass matrix form two orthocentric tetrahedra that share orthocenter coincident with mass center. It is also shown that a realizable stiffness matrix is synthesized by using the orthocentric tetrahedra. Second, the analytical representations for vibration energy produced by a direct (and base) excitation are derived in terms of the vertices of the tetrahedra. These expressions can be used to find vibration modes that satisfy the requirements for the specified work ratios as well as six target resonant frequencies. In conclusion, the systematic design methods are developed to synthesize a spatial system with specific work ratio as well as six target resonant frequencies.

REFERENCES

[1] J. W. Kim, S. Lee, and Y. J. Choi, "Design method of planar vibration system for specified ratio of energy peaks," *J. Sound Vib.*, vol. 344, pp. 363–376, May 2015.
[2] J. Lončarić, "Passive realization of generalized springs," in *Proc. IEEE Int. Symp. Intell. Control*, Arlington, VA, USA, Aug. 1991, pp. 116–121.
[3] S. M. Shahruz, "Design of mechanical band-pass filters for energy scavenging," *J. Sound Vib.*, vol. 292, pp. 987–998, 2006.
[4] M. Ferrari, V. Ferrari, M. Guizzetti, D. Marioli, and A. Taroni, "Piezoelectric multifrequency energy converter for power harvesting in autonomous microsystems," *Sens. Actuators A, Phys.*, vol. 142, pp. 329–335, Mar. 2008.
[5] P. Blanchet, "Linear vibration analysis using screw theory," Ph.D. dissertation, Dept. Mech. Eng., Georgia Inst. Technol., Atlanta, GA, USA, 1998.
[6] M. B. Hong and Y. J. Choi, "Design method of planar three-degrees-of-freedom serial compliance device with desired compliance characteristics," *Proc. Inst. Mech. Eng., C, J. Mech. Eng. Sci.*, vol. 226, no. 9, pp. 2331–2344, Sep. 2012.
[7] H. S. Kim, J. W. Kim, S.-B. Park, and Y. J. Choi, "Design of serial linkage-type vibration energy harvester with three resonant frequencies," *Smart Mater. Struct.*, vol. 26, no. 11, Nov. 2017, Art. no. 115030.
[8] H. S. Kim, W. Ryu, S.-B. Park, and Y. J. Choi, "3-Degree-of-freedom electromagnetic vibration energy harvester with serially connected leaf hinge joints," *J. Intell. Mater. Syst. Struct.*, vol. 30, no. 2, pp. 308–322, Jan. 2019.
[9] R. S. Ball, *A Treatise on the Theory of Screws*. Cambridge, U.K.: Cambridge Univ. Press, 1990.
[10] B. J. Dan and Y. J. Choi, "The geometrical mode and frequency analyses of a vibrating system with planes of symmetry," *J. Sound Vib.*, vol. 241, no. 5, pp. 779–795, Apr. 2001.
[11] B. J. Dan and Y. J. Choi, "Vibration analysis of single rigid-body systems having planes of symmetry," *Proc. Inst. Mech. Eng., C, J. Mech. Eng. Sci.*, vol. 216, no. 6, pp. 629–641, Jun. 2002.
[12] S. J. Jang and Y. J. Choi, "Conditions for the planes of symmetry of an elastically supported rigid body," *Proc. Inst. Mech. Eng., C, J. Mech. Eng. Sci.*, vol. 223, no. 8, pp. 1755–1766, Aug. 2009.
[13] M. B. Hong and Y. J. Choi, "The conditions for mode decoupling of a linear vibration system with diagonalizable stiffness matrices via screw theory," *Proc. Inst. Mech. Eng., C, J. Mech. Eng. Sci.*, vol. 225, no. 1, pp. 101–111, Jan. 2011.
[14] S.-J. Jang, J. W. Kim, and Y. J. Choi, "Triangular relationship between vibration modes of an elastically supported rigid body with a plane of symmetry," *Proc. Inst. Mech. Eng., C, J. Mech. Eng. Sci.*, vol. 226, no. 5, pp. 1254–1262, May 2012.
[15] Y. G. Lee, W. Ryu, H. S. Choi, and Y. J. Choi, "The conditions for a linear vibration system to have only pure rotation modes," *IEEE Access*, vol. 8, pp. 75860–75873, 2020, doi: 10.1109/ACCESS.2020.2988675.
[16] M. Griffis and J. Duffy, "Kinestatic control: A novel theory for simultaneously regulating force and displacement," *J. Mech. Des.*, vol. 113, no. 4, pp. 508–515, Dec. 1991.
[17] N. Ciblak and H. Lipkin, "Synthesis of stiffnesses by springs," in *Proc. ASME Design Eng. Tech. Conf.*, Atlanta, GA, USA, Sep. 1998, pp. 1–10.
[18] S. Huang and J. M. Schimmels, "The bounds and realization of spatial compliances achieved with simple serial elastic mechanisms," *IEEE Trans. Robot. Autom.*, vol. 14, no. 3, pp. 466–475, Jun. 1998.
[19] L. Meirovitch, *Elements of Vibration Analysis*, 2nd ed. New York, NY, USA: McGraw-Hill, 1986.
[20] M. B. Hong and Y. J. Choi, "Screw system approach to physical realization of stiffness matrix with arbitrary rank," *J. Mech. Robot.*, vol. 1, no. 2, pp. 1–8, May 2009.

YEONG GEOL LEE received the B.S. degree in mechanical engineering from Yonsei University, Seoul, South Korea, in 2017, where he is currently pursuing the Ph.D. degree. His main research interests include vibration on the basis of the theory of screws, continuous vibration systems, energy harvesting, and absorbing systems.

YONG JE CHOI received the B.S. degree from Yonsei University, Seoul, South Korea, in 1979, and the M.S. and Ph.D. degrees in robotics from the University of Florida, in 1986 and 1990, respectively. He is currently a Professor with the School of Mechanical Engineering, Yonsei University. His teaching and research interests include applications of screw theory to the design of compliant robotic devices and new theory of vibration.